

Dear Prof. Valerio Lucarini,

Regarding to the initial date of the six prediction systems, we present the details of initial strategy in Table 2. We add a sentence in the caption of Table 2 to clarify the initial date (line 630). The six prediction systems contribute to CMIP5 project, which have been widely used to study climate prediction skill on seasonal-to-decadal scale (Choi et al. 2016; Meehl and Teng 2012; Meehl et al. 2014). Therefore, we employ the six prediction systems to discuss the seasonal prediction skill of east Asian summer monsoon. The six systems have performed a yearly initialisation (line 88-91). The initial date of every prediction year for each prediction system is shown in Table 2. A paragraph in Section 2.1 clarifies why the six prediction systems can be used to study prediction skill on seasonal time-scale (line103-111).

We expect you are agree with our clarification. Thank you very much.

Best regards,

Bo Huang

Choi, J., S. W. Son, Y. G. Ham, J. Y. Lee, and H. M. Kim, 2016: Seasonal-to-Interannual Prediction Skills of Near-Surface Air Temperature in the CMIP5 Decadal Hindcast Experiments. *J Clim*, **29**, 1511-1527.

Meehl, G. A., and H. Y. Teng, 2012: Case studies for initialized decadal hindcasts and predictions for the Pacific region. *Geophys Res Lett*, **39**, L22705.

Meehl, G. A., and Coauthors, 2014: DECADAL CLIMATE PREDICTION An Update from the Trenches. *Bull Am Meteorol Soc*, **95**, 243-267.

# 1 Seasonal Prediction Skill of East Asian Summer Monsoon in CMIP5-Models

2 *Bo Huang,\* Ulrich Cubasch, Christopher Kadow*

3 *Institute of Meteorology, Freie Universität Berlin,*  
4 *Carl-Heinrich-Becker-Weg 6-10, 12165 Berlin, Germany*

5 *Corresponding Author Email: huangb@live.com*

## 7 **ABSTRACT**

8 The East Asian summer monsoon (EASM) is an important part of the global climate system  
9 and plays a vital role in the Asian climate. Its seasonal predictability is a long-standing issue  
10 within the monsoon scientist community. In this study, we ~~will~~ analyse the seasonal (the  
11 leading time is at least six months) prediction skill of the EASM rainfall and its associated  
12 general circulation in non-initialised and initialised simulations for the years 1979-2005  
13 which ~~were~~ are performed by six prediction systems (*i.e.*, the BCC-CSM1-1, the CanCM4,  
14 the GFDL-CM2p1, the HadCM3, the MIROC5 and the MPI-ESM-LR) from the Coupled  
15 Model Intercomparison Project phase 5 (CMIP 5). We ~~find~~ found that most prediction  
16 systems simulated zonal wind over 850 and 200 hPa ~~were~~ are significantly improved in the  
17 initialised simulations compared to non-initialised simulations. Based on the knowledge that  
18 zonal wind indices can be used as potential predictors for the EASM, we ~~selected~~ an EASM  
19 index based upon the zonal wind over 850 hPa for further analysis. This assessment ~~showed~~  
20 shows that the GFDL-CM2p1 and the MIROC5 added prediction skill in simulating the  
21 EASM index with initialisation, the BCC-CSM1-1, the CanCM4, and the MPI-ESM-LR  
22 changed the skill insignificantly, and the HadCM3 ~~indicated~~ indicates a decreased skill score.  
23 The different response to the initialisation can be traced back to the ability of the models to  
24 capture the ENSO (El Niño-Southern Oscillation)-EASM coupled mode, particularly the  
25 Southern Oscillation-EASM coupled mode. As it is known from observational ~~studies~~, this  
26 mode links the oceanic circulation and the EASM rainfall. ~~On the whole~~ Overall, ~~we find that~~  
27 the GFDL-CM2p1 and the MIROC5 are capable ~~of predicting~~ to predict the EASM on a  
28 seasonal time-scale under the current initialisation strategy.

29 **Key Words:** East Asian summer monsoon; initialisation; seasonal prediction; ENSO-EASM  
30 coupled mode; CMIP5

31 1. INTRODUCTION

32 The Asian monsoon is the most powerful monsoon system in the world due to the thermal  
33 contrast between the Eurasian continent and the Indo-Pacific Ocean. Its evolution and  
34 variability critically ~~influences~~influence the livelihood and the socio-economic status of over  
35 two billion people who live in the Asian monsoon dominated region. It encompasses two sub-  
36 monsoon systems, the South Asian monsoon (SAM) and the East Asian monsoon (EAM)  
37 (Wang, 2006). In summer time (June-July-August), the EAM, namely, the East Asian  
38 summer monsoon (EASM) occurs from the Indo-China peninsula to the Korean Peninsula  
39 and Japan, and shows strong intraseasonal-to-interdecadal variability (Ding and Chan, 2005).  
40 Thus, an accurate prediction of the EASM is an important and long-standing issue in climate  
41 science.

42 To predict the EASM, there are two approaches, ~~a~~-statistical prediction and ~~a~~-dynamical  
43 prediction, respectively. The statistical method seeks the relationship between the EASM and  
44 a strong climate signal (e.g., ENSO, NAO; Wu et al., 2009; Yim et al., 2014; Wang et al.,  
45 2015). This method establishes an empirical equation between the EASM and climate index.  
46 However, it is limited by the strength of the climate signal. The other method is ~~a~~-dynamical  
47 prediction. It employs a climate model to predict the EASM (Sperber et al., 2001; Kang and  
48 Yoo, 2006; Wang et al., 2008a; Yang et al., 2008; Lee et al., 2010; Kim et al., 2012). Without  
49 initialisation, both the atmosphere general circulation models (AGCMs) and the coupled  
50 atmosphere-ocean general circulation models (CGCMs) cannot predict the climate on ~~a~~  
51 seasonal time-scale (Goddard et al., 2001). Given an initial condition, the AGCMs have the  
52 ability to predict the climate, but show little skill in predicting the EASM (Wang et al.,  
53 2005; Barnston et al., 2010). Because the AGCMs fail to produce a correct relationship  
54 between the EASM and the sea surface temperature (SST) anomalies over the tropical  
55 western North Pacific, the South China Sea, and the Bay of Bengal (Wang et al., 2004; Wang  
56 et al., 2005), the monsoon community endeavours to predict the EASM with CGCMs (Wang  
57 et al., 2008a; Zhou et al., 2009; Kim et al., 2012; Jiang et al., 2013).

58 CGCMs have proved to be the most valuable tools in predicting the EASM (Wang et al.,  
59 2008a; Zhou et al., 2009; Kim et al., 2012; Jiang et al., 2013). However, the performance of  
60 CGCMs in predicting the EASM on seasonal time-scale strongly depends on their ability to  
61 reproduce the air-sea coupled process (Kug et al., 2008) and on the given initial condition  
62 (Wang et al., 2005). In the coupled model inter-comparison project (CMIP) phase 3 (CMIP3;

63 Meehl et al., 2007) era, the models simulate, not only a too weak tropical SST-monsoon  
64 teleconnection (Kim et al., 2008;Kim et al., 2011), but also a too weak East Asian zonal  
65 wind-rainfall teleconnection (Sperber et al., 2013). Compared to CMIP3 models, CMIP phase  
66 5 (CMIP5; Taylor et al., 2012) models improved the representation of monsoon status  
67 (Sperber et al., 2013). Therefore, given the initial conditions, the CMIP5 models do have the  
68 potential to predict the EASM.

69 As mentioned, initial conditions do play a vital factor in predicting the EASM on sub-  
70 seasonal to seasonal time-scale (Wang et al., 2005;Kang and Shukla, 2006). Under the  
71 current set up of initialisation, the CMIP5 models showed the ability to predict the SST  
72 variation index (*i.e.*, El Niño-Southern Oscillation-ENSO index; Niño3.4) of up to 15 months  
73 in advance (Meehl and Teng, 2012;Meehl et al., 2014;Choi et al., 2016). This extended  
74 prediction skill of the ENSO suggests that the EASM can be predicted on a seasonal time-  
75 scale if the dynamical link between the ENSO and monsoon circulations is well represented  
76 in these models. Two scientific questions will be addressed in this study: 1. How realistic are  
77 the initialised CMIP5 models in representing the EASM? 2. Can the CMIP5 models capture  
78 the dynamical link between the ENSO and EASM?

79 In this paper, we will intercompare the influence of the initialisation on the capability of the  
80 CMIP5 models to capture the EASM and the ENSO-EASM teleconnections. The model  
81 simulations, comparison data and methods are introduced in Section 2. Section 3 describes  
82 the seasonal skill of the rainfall predictions and the prediction of the associated general  
83 circulation of the EASM. The mechanism causing the differential response of the models to  
84 the initialisation is presented in Section 4. The discussions are shown in Section 5. Section 6  
85 summarises the findings of this paper.

## 86 2. MODELS, DATA AND METHODS

### 87 2.1 MODELS AND INITIALISATION

88 In this study, we ~~assessevaluate~~ ed six prediction systems from CMIP5 project (Table 1),  
89 ~~which.~~ ~~The six prediction systems~~ have performed a yearly initialisation (Meehl et al., 2014).  
90 Their simulations can be used in seasonal prediction study. There are two group of  
91 experiments, without initialisation (non-initialisation) and with initialisation, respectively.  
92 For non-initialised simulations, the models ~~were~~ are forced by observed atmospheric  
93 composition changes (reflecting both anthropogenic and natural sources) and, for the first  
94 time, including the time-evolving land cover (Taylor et al., 2012). For initialised simulations,

95 the models update the time-evolving observed atmospheric and oceanic component (Taylor et  
96 al., 2012). Following the CMIP5 framework, the six models established their initialisation  
97 strategy, which are summarised in Table 2. More details about the initialisation strategy of  
98 each model can be found in the reference paper in Table 1. To simplify the comparison, we  
99 select the first lead year (up to 12 months) results for further analysis. The HadCM3-ff is the  
100 full-field initialised simulation, which employs the same CGCM (HadCM3) as the anomaly  
101 initialisation. ~~We select the s~~atellite era (1979 to 2005) simulations are used in the for our  
102 study due to the spatial coverage of precipitation observations.

103 The six models employ different initialisation strategies for atmospheric and oceanic process,  
104 and for initial date (Table 2). These initialisation strategies contribute to a new approach for  
105 climate prediction on decadal time-scale (Meehl et al., 2014). As the ocean is driving the  
106 long-term prediction skill rather than the initial condition of the atmosphere, the timing of the  
107 initialization has to be considered in the time scale of the ocean circulation, i.e. years to  
108 decades. Therefore, on an ocean time scale, the initialization takes place with comparable  
109 timing and therefore the results are comparable. This approach based on decadal prediction  
110 experiments, which deviates from the scores of other seasonal prediction experiments based  
111 on initialisation techniques derived from weather forecasting.

## 112 2.2 COMPARISON DATA

113 The main datasets which ~~were~~are used for comparison in this study include: (1) monthly  
114 precipitation data from the Global Precipitation Climatology Project (GPCP; Adler et al.,  
115 2003); (2) monthly circulation data from ECMWF Interim re-analysis (ERA-Interim; Dee et  
116 al., 2011); and (3) monthly mean SST from National Oceanic and Atmospheric  
117 Administration (NOAA) improved Extended Reconstructed SST version 4 (ERSST v4;  
118 Huang et al., 2015). All the model data and the comparison data are remapped onto a  
119 common grid of 2.5°x2.5° by bi-linear interpolation to reduce the uncertainty induced by  
120 different data resolutions.

## 121 2.3 EAST ASIAN MONSOON INDEX AND ENSO INDEX

122 In recent decades, more than 25 general circulation indices have been produced to define the  
123 variability and the long-term change of the EASM. Wang et al. (2008b) arranged ~~them~~the 25  
124 monsoon indices according to their ability to capture the main features of the EASM. ~~They~~  
125 ~~found that t~~The Wang and Fan index (hereafter WF-index; 1999) ~~showed~~shows the best  
126 performance in capturing the total variance of the precipitation and three-dimensional

127 circulation over East Asia. We, thus, select the WF-index for further analysis. Its definition is  
 128 a standardised average zonal wind at 850 hPa in (5°-15°N, 90°-130°E) minus in (22.5°-  
 129 32.5°N, 110°-140°E). The WF-index is a shear vorticity index which ~~often is~~ described by a  
 130 north-south gradient of the zonal winds. In positive (negative) phase of the WF-index years,  
 131 two strong (weak) rainfall belts located at the Indo China Peninsula-to-the Philippine Sea and  
 132 the northern China-to-the Japanese Sea, and a weak (strong) rainfall belt occurs from the  
 133 Yangtze river basin-to-the south of Japan. The average summer (June-July-August) WF-  
 134 index June-July-August mean of WF index is used to represent the EASM for further  
 135 analysis in this study.

136 Here, we choose the Niño3.4 and southern oscillation index (SOI) to represents the ENSO  
 137 status. The Niño3.4 is calculated by the SST anomaly in the central Pacific (190-240°E, 5°S-  
 138 5°N), while the SOI is based upon the anomaly of the sea level pressure differences between  
 139 Tahiti (210.75°E, 17.6°S) and Darwin (130.83°E, 12.5°S). To calculate the SOI, we  
 140 interpolate the grid data to the Tahiti and the Darwin point by bilinear interpolation.

#### 141 2.4 METHODS

142 In this study, we ~~chose employ~~ the un-centred Pattern Correlation Coefficient (PCC) (for  
 143 more details see Barnett and Schlesinger, 1987) to analyse the model performance in  
 144 comparison ~~to of~~ the observational data, because centred correlations alone are not sufficient  
 145 for the attribution of seasonal prediction (Mitchell et al., 2001). The un-centred PCC is  
 146 defined by:

$$PCC = \frac{\sum_{x=1}^n \sum_{y=1}^m w_{(x,y)} F_{(x,y)} A_{(x,y)}}{\sqrt{\sum_{x=1}^n \sum_{y=1}^m w_{(x,y)} F_{(x,y)}^2 \sum_{x=1}^n \sum_{y=1}^m w_{(x,y)} A_{(x,y)}^2}}$$

147

148 where n and m are grids on longitude and latitude, respectively.  $F_{(x,y)}$  and  $A_{(x,y)}$  represent two  
 149 dimensions comparison and validating value.  $w_{(x,y)}$  indicates the weighting coefficient for  
 150 each grid. An equal weighting coefficient was applied in the study area.

151 We also ~~employed use~~ the anomaly correlation coefficient (ACC) to analyse the model  
 152 performance in reproducing observational variations. The ACC is the correlation between  
 153 anomalies of forecasts and those of verifying values with the reference values, such as  
 154 climatological values (Drosowsky and Zhang, 2003). Its definition is:

$$ACC = \frac{\sum_{i=1}^n w_i (f_i - \bar{f})(a_i - \bar{a})}{\sqrt{\sum_{i=1}^n w_i (f_i - \bar{f})^2 \sum_{i=1}^n w_i (a_i - \bar{a})^2}}, (-1 \leq ACC \leq 1)$$

155

$$f_i = F_i - C_i, \bar{f} = \left( \sum_{i=1}^n w_i f_i \right) / \sum_{i=1}^n w_i$$

156

$$a_i = A_i - C_i, \bar{a} = \left( \sum_{i=1}^n w_i a_i \right) / \sum_{i=1}^n w_i$$

157

158 where  $n$  is the number of samples, and  $F_i$ ,  $A_i$ ,  $C_i$  represent comparison, verifying value, and  
 159 reference value such as climatological value, respectively. Also,  $\bar{f}$  is the mean of  $f_i$ ,  $\bar{a}$  is the  
 160 mean of  $a_i$ , and  $w_i$  indicates the weighting coefficient. If the variation of anomalies of  
 161 comparison dataset is a coincident with that of the anomalies of verifying value, ACC will  
 162 take 1 (the maximum value). It indicates that the forecast has good skill.

163 The root-mean-square-error (RMSE) is employed to check the model deviation from the  
 164 observation and its definition is:

$$RMSE = \sqrt{\sum_{i=1}^n w_i D_i^2} / \sqrt{\sum_{i=1}^n w_i}$$

165

166 where  $D_i$  represents the deviation between comparison and verifying value,  $w_i$  is the  
 167 weighting coefficient for each sample, and  $n$  is the number of samples. If RMSE is closer to  
 168 zero, it means that the comparisons are closer to the verifying values.

### 169 3. SEASONAL PREDICTION SKILL OF THE EASM

170 The EASM has complex spatial and temporal structures that encompass the tropics,  
 171 subtropics, and midlatitudes (Tao and Chen, 1987; Ding, 1994). In the late spring, an  
 172 enhanced rainfall pattern ~~was~~is observed in the Indochina Peninsula and in the South China  
 173 Sea. At the same time, the rainfall belt advances northwards to the south of China. In the  
 174 early summer, the rainfall concentration occurred in the Yangtze River Basin and in southern  
 175 Japan, namely, the Meiyu and Baiu seasons, respectively. The rainfall belt can reach as far as  
 176 northern China, the Korean Peninsula (called the Changma rainy season) and central Japan in  
 177 July (Ding, 2004; Ding and Chan, 2005).

178 The EASM is characterised by both seasonal heterogeneous rainfall distribution and  
179 associated large-scale circulation systems (Wang et al., 2008b). In the summer season, water  
180 moisture migrates from the Pacific Ocean to central and eastern Asia, which is carried by the  
181 southwest surface winds. Generally, a strong summer monsoon year is followed by  
182 precipitation in northern China, while a weak summer monsoon year is usually accompanied  
183 by heavier rainfall along the Yangtze River basin (Ding, 1994; Zhou and Yu, 2005).

184 For multi-model ensemble mean (MME), the prediction skill of the June-July-August mean  
185 rainfall and the associated general circulation variable (*i.e.*, zonal and meridional wind, and  
186 mean sea level pressure) is presented in Figure 1. These variables have been widely used to  
187 calculate the monsoon index (Wang et al., 2008b). Table 3 shows the contribution of these  
188 variables in the EASM. Their abbreviations follow the guidelines of CMIP5 (Taylor et al.,  
189 2012). Compared to the non-initialised experiment, a larger predicted area can be found in the  
190 initialised experiment, especially for the psl, ua850 and ua200. There are small changes to the  
191 predicted area between the non-initialised and initialised experiment for the pr, va850 and  
192 va200. The individual model shows an acceptable performance (high PCC) in capturing the  
193 observed spatial variation of the six variables, but a poor performance in simulating their  
194 temporal variation (with low ACC) (Figure 2). There is no improvement in estimating the  
195 spatial variation of the six variables with initialisation. We can see that the models show a  
196 higher ACC in the initialised simulations than that in the non-initialised ones. The  
197 improvement of simulating the temporal variation of zonal winds (*i.e.*, ua850 and ua200) is  
198 larger than that of the rainfall and meridional winds. One can exploit this improvement by  
199 using a general circulation based monsoon index as a tool to predict the EASM. As  
200 mentioned in section 2.3, the WF-index better represents the monsoon rainfall and its  
201 associated general circulation structure than the other monsoon index. Therefore, the  
202 prediction skill of EASM in the following analysis is based on the WF-index.

203 In non-initialised simulations, none of the models captured the observed EASM, as indicated  
204 by an insignificant ACC (Figure 3). The CanCM4 and the GFDL-CM2p1 simulate a negative  
205 phase, while the BCC-CSM1-1, the HadCM3, the MIROC5 and the MPI-ESM-LR all  
206 predicted a positive phase of the EASM. With initialisation, the GFDL-CM2p1 and the  
207 MIROC5 improved the skill to simulate the EASM, the CanCM4 and the MPI-ESM-LR  
208 displayed hardly any reaction, while the BCC-CSM1-1 and the HadCM3 showed a worse  
209 performance than without initialisation. Particularly with anomaly initialisation, the HadCM3



210 significantly lost its prediction skill in capturing the EASM. The CMIP5 models showed  
211 different response to the initialisation in predicting the EASM on seasonal time-scale. To  
212 understand the potential reason, we analysed the principle components of six variables,  
213 which contributed to the EASM. The details are presented in Section 4.

#### 214 4. EASM-ENSO COUPLED MODE IN CMIP5

215 We employed the EOF method to analyse the leading EOF modes of the six meteorological  
216 variables anomaly in the EASM region ( $0^{\circ}$ - $50^{\circ}$ N,  $100^{\circ}$ - $140^{\circ}$ E). The first EOF mode of the  
217 rainfall is characterised by a “sandwich” pattern, which showed sharp contrast between the  
218 prominent rainfall centre over Malaysia, the Yangtze River valley and the south of Japan, and  
219 the enhanced rainfall over the Indo-China Peninsula and the Philippine Sea (Figure 4). The  
220 increased precipitation is associated with cyclones in the low-level (850 hPa) and anti-  
221 cyclones in the upper level (200 hPa).

222 The correlation coefficient of the first eigenvector and the associated principal component  
223 (PC) between the model simulation and the observation in the non-initialised and the  
224 initialised simulation is presented in Figure 5. The models captured the eigenvector of the  
225 first EOF for the six meteorological fields in non-initialised simulation. However, they failed  
226 to reproduce the associated PC of the first leading EOF mode. Compared to the non-  
227 initialised simulation, the models showed no improvement to simulate the first leading EOF  
228 mode of rainfall, but exhibit a better performance in representing the first leading EOF mode  
229 of zonal wind. The CanCM4 and the GFDL-CM2p1 captured the first PC of ua850, but not  
230 the other five models. For the zonal wind at 200 hPa, the BCC-CSM1-1 fails to simulate its  
231 first EOF mode while the other six models can. Only the GFDL-CM2p1 accurately simulates  
232 the first EOF eigenvectors and the associated PC of va850, which cannot be reproduced in the  
233 other models. No models captured the spatial-temporal variation of the first EOF mode of  
234 meridional wind at 200 hPa. In addition, the GFDL-CM2p1 and the MIROC5 simulate a  
235 reasonable leading EOF mode and associated PC of psl, while the other models do not  
236 capture it.

237 Figure 6 shows the fractional (percentage) variances of the six variables from the first EOF  
238 mode with the total variances from the observation, and the model simulation with (with-out)  
239 initialisation. The observational total variances for the pr, the ua850, the ua200, the va850,  
240 the va200 and the psl, are depicted by the first lead EOF mode in 21.2, 59.0, 36.5, 20.6, 28.5  
241 and 50.0 percent, respectively. The prediction systems models simulated the comparable

242 ~~explanatory variance~~ a comparable explanatory variance, which showed a slight discrepancy  
243 for the first leading mode in the non-initialisation. From non-initialised simulation to  
244 initialised simulation, the ~~CGCMs-prediction systems~~ tended to enhance the first EOF leading  
245 mode because they show larger fractional variances of the total variances of ~~the~~ six variables.  
246 We note that the CanCM4 and the GFDL-CM2p1 significantly increased the fractional  
247 variances from non-initialisation to initialisation.

248 The ENSO is a dominant mode of the inter-annual variability of the coupled ocean and  
249 atmosphere climate system, which has strong effects on the inter-annual variation of the  
250 EASM (Wang et al., 2000; Wu et al., 2003). Wang et al. (2015) summarised that the first EOF  
251 lead mode of the ASM is ENSO developing mode. As previously mentioned, the first EOF  
252 mode ~~is~~ was improved in the initialised simulations, compared to the non-initialised  
253 simulation. This also can be found in the ENSO indices (Figure 7). The individual members  
254 and their ensemble mean of the six models show a low correlation coefficient to the  
255 observational Niño3.4 and the SOI in the non-initialised simulations. ~~These~~ two indices  
256 showed strong anti-phases in the observation, with the correlation range being -0.94 to -0.92  
257 for four seasons (DJF, MAM, JJA, SON). Without initialisation, the models can describe the  
258 anti-correlation between Niño3.4 and the SOI, but with a weaker correlation. Compared to  
259 the non-initialisation, there is a significant improvement for models in capturing the  
260 observation ~~of~~ Niño3.4 and the SOI in the initialised experiments. The initialisation lowers  
261 the spread of Niño3.4 and the SOI in all the six models. There is a noticeable change between  
262 the model in producing the relationship between the Niño3.4 and the SOI. We ~~found~~ that  
263 the GFDL-CM2p1 (HadCM3) shows a lower (higher) Niño3.4-SOI correlation in  
264 ~~initialisation~~ initialised than that in non-initialised simulations. With initialisation, the  
265 ensemble mean of each model outperforms its individual members in capturing Niño3.4 and  
266 the SOI, while without initialisation it showed a worse performance than that of the  
267 individual members in simulating Niño3.4 and the SOI.

268 The EASM strongly relies on the pre-seasons ENSO signal due to the lag response of the  
269 atmosphere to the SST anomaly (Wu et al., 2003). The lead-lag correlation coefficients  
270 between the EASM index and the Niño3.4, and the SOI from JJA(-1) to JJA(+1) are  
271 illustrated in Figure 8. The pre-season Niño3.4 (SOI) presents a significant negative  
272 (positive) correlation to the EASM, while the post-season Niño3.4 (SOI) showed a notable  
273 positive (negative) correlation. This lead-lag correlation coefficient phase is called the

274 Niño3.4-/SOI-EASM coupled mode (Wang et al., 2008b). In the non-initialised cases, the  
275 models do not produce the teleconnection between the ENSO and the EASM. The CanCM4,  
276 the HadCM3 and the MPI-ESM-LR failed to represent the lead-lag correlation coefficient  
277 differences between pre-/post-season ENSO and EASM. The BCC-CSM1-1, the GFDL-  
278 CM2p1 and the MIROC5 capture the coupled mode of the ENSO and the EASM. However,  
279 the pre-season ENSO has a weak effect on the EASM. Compared to the non-initialised cases,  
280 the MIROC5 and the GFDL-CM2p1 both demonstrated a significant improvement in  
281 simulating Niño3.4 (SOI)-EASM coupled mode in the initialisation. The BCC-CSM1-1, the  
282 HadCM3, and the HadCM3-ff showed no improvement, with insignificant correlation  
283 between Niño3.4 (SOI) and the EASM. The CanCM4 and the MPI-ESM-LR indicated a  
284 higher correlation between the EASM and the simultaneous-to-post-season ENSO than to the  
285 pre-season ENSO.

## 286 5. DISCUSSION

287 The model exhibits a better performance in simulating the general circulation of the EASM  
288 with initialisation. Thus, initialisation is helpful in forecasting the EASM on a seasonal time-  
289 scale. There are two initialisation methods in our study, full-field initialisation and anomaly  
290 initialisation (Table 1). The full-field initialisation produces more skilful predictions on the  
291 seasonal time-scale in predicting regional temperature and precipitation (Magnusson et al.,  
292 2013;Smith et al., 2013). Nevertheless, for predicting the EASM, there is no significant  
293 difference between the two methods. We can see that both the GFDL-CM2p1 and the  
294 MIROC5 have a significant improvement in capturing the EASM, with full-field and  
295 anomaly initialisation, respectively. Only the HadCM3 was is initialised by the two  
296 initialisation techniques. However, both these two initialised techniques are producing poor  
297 predictions of the EASM with no major differences.

298 The current initialisation strategy updates the observed atmospheric component (*i.e.*, zonal  
299 and meridional wind, geopotential height, *etc.*) and the SST (Meehl et al., 2009;Taylor et al.,  
300 2012;Meehl et al., 2014). With initialisation, the SST conveys its information via the large  
301 heat content of the ocean to the coupled system. Therefore, an index indicating an ocean  
302 oscillation like Niño3.4 show a seasonal-to-decadal prediction skill (Jin et al., 2008;Luo et  
303 al., 2008;Choi et al., 2016). The models studied study here demonstrated a prediction skill in  
304 simulating Niño3.4 and the SOI due to this effect. The change of the correlation between  
305 Niño3.4 and the SOI is insignificant from non-initialised to initialised simulations. We

306 therefore conclude that the relationship between Niño3.4 and the SOI ~~more~~ depends ~~more~~ on  
307 the model parameterisation than on the initial condition.

308 Wang *et al.* (2015) found that the second EOF mode of ASM is the Indo-western Pacific  
309 monsoon-ocean coupled mode, the third is the Indian Ocean dipole (IOD) mode, and the  
310 fourth is the trend mode. The Indo-western Pacific monsoon-ocean coupled mode is the  
311 atmosphere-ocean interaction mode (Wang *et al.*, 2013; Xiang *et al.*, 2013), which is  
312 supported by a positive thermodynamic feedback between the western North Pacific (WNP)  
313 anticyclone and the underlying Indo-Pacific sea surface temperature anomaly dipole over the  
314 warm pool (Wang *et al.*, 2015). The IOD increases the precipitation from the South Asian  
315 subcontinent to southeastern China and suppresses the precipitation over the WNP (Wang *et al.*  
316 *et al.*, 2015). It affects the Asian monsoon by the meridional asymmetry of the monsoonal  
317 easterly shear during the boreal summer, which can particularly strengthen the northern  
318 branch of the Rossby wave response to the south-eastern Indian Ocean SST cooling, leading  
319 to an intensified monsoon flow as well as an intensified convection (Wang and Xie,  
320 1996; Wang *et al.*, 2003; Xiang *et al.*, 2011; Wang *et al.*, 2015). We noted that the models  
321 simulate a reasonable first EOF mode, but illustrate no skill in capturing the other EOF  
322 leading modes (not shown). We argue that the models cannot well represent the monsoon-  
323 ocean interaction, even with initialisation. The models do not simulate the third EOF leading  
324 mode of the EASM since the predictability of the IOD extends only over a three-month time-  
325 scale (Choudhury *et al.*, 2015). The current initialisation strategies (both anomaly and full  
326 field) enhance the ENSO signal in the model simulations with higher explained fraction of  
327 variance. Kim *et al.* (2012) described a similar finding in ECMWF System 4 and NCEP  
328 Climate Forecast System version 2 (CFSv2) seasonal prediction simulations. With  
329 initialisation, the models well predict ENSO on seasonal time-scale, which leads to an overly  
330 strong modulation of the EASM by ENSO (Jin *et al.*, 2008; Kim *et al.*, 2012).

331 It is worth mentioning that it ~~was-is~~ an extremely weak monsoon and strong El Niño year in  
332 1998. The CanCM4, the GFDL-CM2p1, the MIROC5 and the MPI-ESM-LR have the ability  
333 to simulate the extreme monsoon event, while the BCC-CSM1-1, and the HadCM3 do not  
334 capture it even with initialisation. There is the potential for the BCC-CSM and the HadCM  
335 models to improve the teleconnection between the ENSO and the EASM.

336 This study ~~has-discussed~~discusses six CMIP5 models in predicting the EASM on seasonal  
337 time-scale. The six models are earth system coupled models which present a better SST-

338 monsoon teleconnection than CMIP3 models (Sperber et al., 2013) and IRI (International  
339 Research Institute for Climate and Society) models (Barnston et al., 2010). There are 4  
340 AGCMs contributing to the IRI prediction system, including ECHAM4.5, CCM3.6, COLA  
341 and GFDL-AM2p14. These models are forced to forecast the climate on seasonal time-scale  
342 by prescribed SST. Barnston et al. (2010) found that the models showed low prediction skill  
343 over East Asia. Therefore, the IRI prediction system cannot be used to predict the EASM.  
344 There are two seasonal forecast application systems, the ECMWF System and the NCEP  
345 CFS, respectively. Both the two application systems have low prediction skill of EASM (Kim  
346 et al., 2012;Jiang et al., 2013). The CMIP5 models have potential to be developed as  
347 application system for EASM seasonal prediction, especially the GFDL-CM2p1 and the  
348 MIROC5.

349 To better predict the short-to-long term climate, World Climate Research Programme  
350 (WCRP) launched two new projects, i.e., Climate-system Historical Forecast Project (CHFP;  
351 Kirtman and Pirani, 2009;Tompkins et al., 2017) and Subseasonal-to-Seasonal (S2S)  
352 Prediction Project (Vitart et al., 2017). The two projects coordinate most climate modelling  
353 research group and provide a large range of forecast dataset. A comprehensive comparison of  
354 all the CHFP and S2S data with the CMIP5 simulations regard to the seasonal prediction skill  
355 of the EASM is certainly an interesting topic, which should be addressed in an additional  
356 paper.

357 We have compared six CMIP5 systems with their respective initialisation strategies. The  
358 GFDL-CM2p1 and the MIROC5 have the potential to serve as seasonal forecast application  
359 system even with their current initialisation method. These models have great potential to  
360 optimise the SST-EASM interaction simulation performance to improve their seasonal  
361 prediction skill of the EASM.

## 362 6. SUMMARY

363 Six earth system models from CMIP5 have been selected in this study. We have analysed the  
364 improvement of the rainfall, the mean sea level pressure, the zonal wind and the meridional  
365 wind in the EASM region from non-initialisation to initialisation. The low prediction skill of  
366 the summer monsoon precipitation is due to the uncertainties of cloud physics and cumulus  
367 parameterisations in the models (Lee et al., 2010;Seo et al., 2015). The models show ~~ed~~-a  
368 better performance in capturing the inter-annual variability of zonal wind than the  
369 precipitation ~~after~~-with initialisation. Thus, the zonal wind index is an additional factor,

370 which can indicate the prediction skill of the model. When, we calculate the WF-index in  
371 both non-initialised and initialised simulations, the GFDL-CM2p1 and the MIROC5 showed  
372 a significant advancement in simulating the EASM from non-initialised to initialised  
373 simulation with a lower RMSE and a higher ACC. There is ~~only~~ a slight change in the WF-  
374 index calculated from the BCC-CSM1-1, the CanCM4 and the MPI-ESM-LR data with  
375 initialisation. Compared to the non-initialised simulation, the HadCM3 loses prediction skill,  
376 especially with anomaly initialisation.

377 To test the possible mechanisms of the models' performance in the non-initialisation and the  
378 initialisation, we have calculated the leading mode of the six fields, which are associated to  
379 the EASM. The models demonstrated a better agreement with the observational first EOF  
380 mode in the initialised simulations. The first lead mode of zonal wind at 200 hPa showed a  
381 significant improvement in the models except the BCC-CSM1-1 with initialisation.  
382 Therefore, a potential predictor might be an index based upon the zonal wind at 200 hPa.  
383 Compared to the non-initialisation, the models enhanced the first EOF mode with a higher  
384 fraction of variance to the total variance after initialisation. The first EOF mode of the EASM  
385 is the ENSO developing mode (Wang et al., 2015). We have analysed the seasonal simulating  
386 skill of Niño3.4 and the SOI in each model. The models showed a poor performance in  
387 representing Niño3.4 and the SOI in the non-initialised simulation. Initialisation ~~improved~~  
388 improves the model simulating skill of Niño3.4 and the SOI. The initialised simulations  
389 decreased the spread of ensemble members in the models. We ~~found~~ find that there is no  
390 significant change in the models reproducing the correlation between Niño3.4 and the SOI  
391 from non-initialisation to initialisation.

392 In general, the pre-season warm phase of the ENSO (El Niño) leads to a weak EASM  
393 producing more rainfall over the South China Sea and northwest China, and less rainfall over  
394 the Yangtze River Valley and the southern Japan; the cold phase of the ENSO (La Niña)  
395 illustrated a reverse rainfall pattern to El Niño in East Asia. The pre-season Niño3.4 (SOI)  
396 exhibits a strong negative (positive) correlation to the EASM, while the correlation between  
397 the post-season Niño3.4 (SOI) and the EASM illustrated an anti-phase as the pre-season. In  
398 the non-initialised simulations, the models do not capture Niño3.4-/SOI-EASM coupled  
399 mode. ~~We found that only~~ The MIROC5 is the only one model has the ability to represent  
400 the Niño3.4-EASM coupled mode with initialisation. For the SOI-EASM coupled mode, the  
401 GFDL-CM2p1 and the MIROC5 ~~captured~~ capture it in the initialisation, while the BCC-

402 CSM1-1, the HadCM3, the HadCM2-ff, the CanCM4 and the MPI-ESM-LR do not.  
403 Therefore, we argue that the differential depiction of ENSO-EASM coupled mode in CMIP5  
404 models lead to their differential response to initialisation.

#### 405 **Acknowledgements**

406 The China Scholarship Council (CSC) and the Freie Universität Berlin supported this work.  
407 We would like to thank the climate modelling groups listed in Table 1 of this paper for  
408 producing and making their model output available. We acknowledge the MiKlip project  
409 funded by the Federal Ministry of Education and Research and the German Climate  
410 Computing Centre (DKRZ) and the HPC Service of ZEDAT for providing the data services.  
411 We are grateful to Mrs Margerison Patricia for her useful comments and the proofreading  
412 work on this manuscript. Authors thank two anonymous reviewers for their useful inputs to  
413 the manuscript.

#### 414 **References**

- 415 Adler, R. F., Huffman, G. J., Chang, A., Ferraro, R., Xie, P.-P., Janowiak, J., Rudolf, B.,  
416 Schneider, U., Curtis, S., Bolvin, D., Gruber, A., Susskind, J., Arkin, P., and Nelkin, E.: The  
417 Version-2 Global Precipitation Climatology Project (GPCP) Monthly Precipitation Analysis  
418 (1979–Present), *J Hydrometeorol*, 4, 1147-1167, 10.1175/1525-  
419 7541(2003)004<1147:tvvgpcp>2.0.co;2, 2003.
- 420 Arora, V. K., Scinocca, J. F., Boer, G. J., Christian, J. R., Denman, K. L., Flato, G. M.,  
421 Kharin, V. V., Lee, W. G., and Merryfield, W. J.: Carbon emission limits required to satisfy  
422 future representative concentration pathways of greenhouse gases, *Geophys Res Lett*, 38,  
423 L05805, 10.1029/2010gl046270, 2011.
- 424 Barnett, T. P., and Schlesinger, M. E.: Detecting Changes in Global Climate Induced by  
425 Greenhouse Gases, *J Geophys Res Atmos*, 92, 14772-14780, 10.1029/JD092iD12p14772,  
426 1987.
- 427 Barnston, A. G., Li, S. H., Mason, S. J., DeWitt, D. G., Goddard, L., and Gong, X. F.:  
428 Verification of the First 11 Years of IRI's Seasonal Climate Forecasts, *J Appl Meteorol Clim*,  
429 49, 493-520, 10.1175/2009jamc2325.1, 2010.
- 430 Choi, J., Son, S. W., Ham, Y. G., Lee, J. Y., and Kim, H. M.: Seasonal-to-Interannual  
431 Prediction Skills of Near-Surface Air Temperature in the CMIP5 Decadal Hindcast  
432 Experiments, *J Clim*, 29, 1511-1527, 10.1175/Jcli-D-15-0182.1, 2016.
- 433 Choudhury, D., Sharma, A., Sivakumar, B., Sen Gupta, A., and Mehrotra, R.: On the  
434 predictability of SSTA indices from CMIP5 decadal experiments, *Environ Res Lett*, 10,  
435 074013, 10.1088/1748-9326/10/7/074013, 2015.
- 436 Dee, D. P., Uppala, S. M., Simmons, A. J., Berrisford, P., Poli, P., Kobayashi, S., Andrae, U.,  
437 Balmaseda, M. A., Balsamo, G., Bauer, P., Bechtold, P., Beljaars, A. C. M., van de Berg, L.,  
438 Bidlot, J., Bormann, N., Delsol, C., Dragani, R., Fuentes, M., Geer, A. J., Haimberger, L.,  
439 Healy, S. B., Hersbach, H., Holm, E. V., Isaksen, L., Kallberg, P., Kohler, M., Matricardi, M.,  
440 McNally, A. P., Monge-Sanz, B. M., Morcrette, J. J., Park, B. K., Peubey, C., de Rosnay, P.,  
441 Tavolato, C., Thepaut, J. N., and Vitart, F.: The ERA-Interim reanalysis: configuration and  
442 performance of the data assimilation system, *Q J R Meteorolog Soc*, 137, 553-597,  
443 10.1002/qj.828, 2011.

444 Delworth, T. L., Broccoli, A. J., Rosati, A., Stouffer, R. J., Balaji, V., Beesley, J. A., Cooke,  
445 W. F., Dixon, K. W., Dunne, J., Dunne, K. A., Durachta, J. W., Findell, K. L., Ginoux, P.,  
446 Gnanadesikan, A., Gordon, C. T., Griffies, S. M., Gudgel, R., Harrison, M. J., Held, I. M.,  
447 Hemler, R. S., Horowitz, L. W., Klein, S. A., Knutson, T. R., Kushner, P. J., Langenhorst, A.  
448 R., Lee, H. C., Lin, S. J., Lu, J., Malyshev, S. L., Milly, P. C. D., Ramaswamy, V., Russell, J.,  
449 Schwarzkopf, M. D., Shevliakova, E., Sirutis, J. J., Spelman, M. J., Stern, W. F., Winton, M.,  
450 Wittenberg, A. T., Wyman, B., Zeng, F., and Zhang, R.: GFDL's CM2 global coupled climate  
451 models. Part I: Formulation and simulation characteristics, *J Clim*, 19, 643-674,  
452 10.1175/Jcli3629.1, 2006.

453 Ding, Y.: Seasonal march of the East-Asian summer monsoon., in: *East Asian Monsoon*,  
454 edited by: Chang, C.-P., World Scientific, Singapore, 560, 2004.

455 Ding, Y. H.: *Monsoons over China*, Kluwer Academic Publisher, Dordrecht/Boston/London,  
456 419 pp., 1994.

457 Ding, Y. H., and Chan, J. C. L.: The East Asian summer monsoon: an overview, *Meteorol*  
458 *Atmos Phys*, 89, 117-142, 10.1007/s00703-005-0125-z, 2005.

459 Drosowsky, W., and Zhang, H.: Verification of Spatial Fields, in: *Forecast Verification: A*  
460 *Practitioner's Guide in Atmospheric Science* edited by: Jolliffe, L. T., and Stephenson, D. B.,  
461 John Wiley & Sons Ltd, England, 128-129, 2003.

462 Goddard, L., Mason, S. J., Zebiak, S. E., Ropelewski, C. F., Basher, R., and Cane, M. A.:  
463 Current approaches to seasonal-to-interannual climate predictions, *Int J Climatol*, 21, 1111-  
464 1152, 10.1002/joc.636, 2001.

465 Huang, B. Y., Banzon, V. F., Freeman, E., Lawrimore, J., Liu, W., Peterson, T. C., Smith, T.  
466 M., Thorne, P. W., Woodruff, S. D., and Zhang, H. M.: Extended Reconstructed Sea Surface  
467 Temperature Version 4 (ERSST.v4). Part I: Upgrades and Intercomparisons, *J Clim*, 28, 911-  
468 930, 10.1175/Jcli-D-14-00006.1, 2015.

469 Jiang, X. W., Yang, S., Li, Y. Q., Kumar, A., Liu, X. W., Zuo, Z. Y., and Jha, B.: Seasonal-  
470 to-Interannual Prediction of the Asian Summer Monsoon in the NCEP Climate Forecast  
471 System Version 2, *J Clim*, 26, 3708-3727, 10.1175/Jcli-D-12-00437.1, 2013.

472 Jin, E. K., Kinter, J. L., Wang, B., Park, C. K., Kang, I. S., Kirtman, B. P., Kug, J. S., Kumar,  
473 A., Luo, J. J., Schemm, J., Shukla, J., and Yamagata, T.: Current status of ENSO prediction  
474 skill in coupled ocean-atmosphere models, *Clim Dyn*, 31, 647-664, 10.1007/s00382-008-  
475 0397-3, 2008.

476 Kang, I.-S., and Shukla, J.: Dynamic seasonal prediction and predictability of the monsoon,  
477 in: *The Asian Monsoon*, edited by: Wang, B., Springer Berlin Heidelberg, Berlin, Heidelberg,  
478 585-612, 2006.

479 Kang, I. S., and Yoo, J. H.: Examination of multi-model ensemble seasonal prediction  
480 methods using a simple climate system, *Clim Dyn*, 26, 285-294, 10.1007/s00382-005-0074-8,  
481 2006.

482 Kim, H. J., Wang, B., and Ding, Q. H.: The Global Monsoon Variability Simulated by  
483 CMIP3 Coupled Climate Models, *J Clim*, 21, 5271-5294, 10.1175/2008jcli2041.1, 2008.

484 Kim, H. J., Takata, K., Wang, B., Watanabe, M., Kimoto, M., Yokohata, T., and Yasunari, T.:  
485 Global Monsoon, El Nino, and Their Interannual Linkage Simulated by MIROC5 and the  
486 CMIP3 CGCMs, *J Clim*, 24, 5604-5618, 10.1175/2011jcli4132.1, 2011.

487 Kim, H. M., Webster, P. J., Curry, J. A., and Toma, V. E.: Asian summer monsoon prediction  
488 in ECMWF System 4 and NCEP CFSv2 retrospective seasonal forecasts, *Clim Dyn*, 39,  
489 2975-2991, 10.1007/s00382-012-1470-5, 2012.

490 Kirtman, B., and Pirani, A.: The State of the Art of Seasonal Prediction Outcomes and  
491 Recommendations from the First World Climate Research Program Workshop on Seasonal  
492 Prediction, *Bull Am Meteorol Soc*, 90, 455-458, 10.1175/2008bams2707.1, 2009.



493 Kug, J. S., Kang, I. S., and Choi, D. H.: Seasonal climate predictability with Tier-one and  
494 Tier-two prediction systems, *Clim Dyn*, 31, 403-416, DOI 10.1007/s00382-007-0264-7, 2008.

495 Lee, J.-Y., Wang, B., Kang, I. S., Shukla, J., Kumar, A., Kug, J. S., Schemm, J. K. E., Luo, J.  
496 J., Yamagata, T., Fu, X., Alves, O., Stern, B., Rosati, T., and Park, C. K.: How are seasonal  
497 prediction skills related to models' performance on mean state and annual cycle?, *Clim Dyn*,  
498 35, 267-283, 10.1007/s00382-010-0857-4, 2010.

499 Luo, J.-J., Masson, S., Behera, S. K., and Yamagata, T.: Extended ENSO Predictions Using a  
500 Fully Coupled Ocean–Atmosphere Model, *J Clim*, 21, 84-93, 10.1175/2007jcli1412.1, 2008.

501 Magnusson, L., Alonso-Balmaseda, M., Corti, S., Molteni, F., and Stockdale, T.: Evaluation  
502 of forecast strategies for seasonal and decadal forecasts in presence of systematic model  
503 errors, *Clim Dyn*, 41, 2393-2409, 10.1007/s00382-012-1599-2, 2013.

504 Matei, D., Pohlmann, H., Jungclaus, J., Muller, W., Haak, H., and Marotzke, J.: Two Tales of  
505 Initializing Decadal Climate Prediction Experiments with the ECHAM5/MPI-OM Model, *J  
506 Clim*, 25, 8502-8523, 10.1175/Jcli-D-11-00633.1, 2012.

507 Meehl, G., Covey, C., Delworth, T., Latif, M., McAvaney, B., Mitchell, J., Stouffer, R., and  
508 Taylor, K.: The WCRP CMIP3 multi-model dataset: a new era in climate change research,  
509 *Bull Am Meteorol Soc*, 88, 1383-1394, 2007.

510 Meehl, G. A., Goddard, L., Murphy, J., Stouffer, R. J., Boer, G., Danabasoglu, G., Dixon, K.,  
511 Giorgetta, M. A., Greene, A. M., Hawkins, E., Hegerl, G., Karoly, D., Keenlyside, N.,  
512 Kimoto, M., Kirtman, B., Navarra, A., Pulwarty, R., Smith, D., Stammer, D., and Stockdale,  
513 T.: DECADAL PREDICTION Can It Be Skillful?, *Bull Am Meteorol Soc*, 90, 1467-1485,  
514 10.1175/2009bams2778.1, 2009.

515 Meehl, G. A., and Teng, H. Y.: Case studies for initialized decadal hindcasts and predictions  
516 for the Pacific region, *Geophys Res Lett*, 39, L22705, 10.1029/2012gl053423, 2012.

517 Meehl, G. A., Goddard, L., Boer, G., Burgman, R., Branstator, G., Cassou, C., Corti, S.,  
518 Danabasoglu, G., Doblas-Reyes, F., Hawkins, E., Karspeck, A., Kimoto, M., Kumar, A.,  
519 Matei, D., Mignot, J., Msadek, R., Navarra, A., Pohlmann, H., Rienecker, M., Rosati, T.,  
520 Schneider, E., Smith, D., Sutton, R., Teng, H. Y., van Oldenborgh, G. J., Vecchi, G., and  
521 Yeager, S.: DECADAL CLIMATE PREDICTION An Update from the Trenches, *Bull Am  
522 Meteorol Soc*, 95, 243-267, 10.1175/Bams-D-12-00241.1, 2014.

523 Mitchell, J. F. B., Karoly, D. J., Hegerl, G. C., Zwiers, F. W., Allen, M. R., and Marengo, J.:  
524 Detection of Climate Change and Attribution of Causes, in: *Third Assessment Report of the  
525 Intergovernmental Panel on Climate Change.*, edited by: Houghton, J. T., Griggs, D. J.,  
526 Noguer, M., van der Linden, P. J., Dai, X., Maskell, K., and Johnson, C. A., Cambridge  
527 University Press, New York, 470, 2001.

528 Seo, K. H., Son, J. H., Lee, J. Y., and Park, H. S.: Northern East Asian Monsoon Precipitation  
529 Revealed by Airmass Variability and Its Prediction, *J Clim*, 28, 6221-6233, 10.1175/Jcli-D-  
530 14-00526.1, 2015.

531 Smith, D. M., Eade, R., and Pohlmann, H.: A comparison of full-field and anomaly  
532 initialization for seasonal to decadal climate prediction, *Clim Dyn*, 41, 3325-3338,  
533 10.1007/s00382-013-1683-2, 2013.

534 Sperber, K., Annamalai, H., Kang, I. S., Kitoh, A., Moise, A., Turner, A., Wang, B., and  
535 Zhou, T.: The Asian summer monsoon: an intercomparison of CMIP5 vs. CMIP3 simulations  
536 of the late 20th century, *Clim Dyn*, 41, 2711-2744, 10.1007/s00382-012-1607-6, 2013.

537 Sperber, K. R., Brankovic, C., Deque, M., Frederiksen, C. S., Graham, R., Kitoh, A.,  
538 Kobayashi, C., Palmer, T., Puri, K., Tennant, W., and Volodin, E.: Dynamical seasonal  
539 predictability of the Asian summer monsoon, *Mon Weather Rev*, 129, 2226-2248,  
540 10.1175/1520-0493(2001)129<2226:Dspota>2.0.Co;2, 2001.

541 Tao, S. Y., and Chen, L. X.: A review of recent research on the East Asian summer monsoon  
542 in China, in: Monsoon Meteorology, edited by: Chang, C.-P., and Krishnamurti, T. N., Oxford  
543 University Press, Oxford, 60-92, 1987.

544 Tatebe, H., Ishii, M., Mochizuki, T., Chikamoto, Y., Sakamoto, T. T., Komuro, Y., Mori, M.,  
545 Yasunaka, S., Watanabe, M., Ogochi, K., Suzuki, T., Nishimura, T., and Kimoto, M.: The  
546 Initialization of the MIROC Climate Models with Hydrographic Data Assimilation for  
547 Decadal Prediction, *J Meteorol Soc Japan*, 90a, 275-294, 10.2151/jmsj.2012-A14, 2012.

548 Taylor, K. E., Stouffer, R. J., and Meehl, G. A.: An Overview of CMIP5 and the Experiment  
549 Design, *Bull Am Meteorol Soc*, 93, 485-498, 10.1175/Bams-D-11-00094.1, 2012.

550 Tompkins, A. M., Ortiz De Zarate, M. I., Saurral, R. I., Vera, C., Saulo, C., Merryfield, W. J.,  
551 Sigmond, M., Lee, W. S., Baehr, J., Braun, A., Butler, A., Deque, M., Doblas-Reyes, F. J.,  
552 Gordon, M., Scaife, A. A., Imada, Y., Ishii, M., Ose, T., Kirtman, B., Kumar, A., Muller, W.  
553 A., Pirani, A., Stockdale, T., Rixen, M., and Yasuda, T.: The Climate-System Historical  
554 Forecast Project: Providing Open Access to Seasonal Forecast Ensembles from Centers  
555 around the Globe, *Bull Am Meteorol Soc*, 98, 2293-2302, 10.1175/Bams-D-16-0209.1, 2017.

556 Vitart, F., Ardilouze, C., Bonet, A., Brookshaw, A., Chen, M., Codorean, C., Deque, M.,  
557 Ferranti, L., Fucile, E., Fuentes, M., Hendon, H., Hodgson, J., Kang, H. S., Kumar, A., Lin,  
558 H., Liu, G., Liu, X., Malguzzi, P., Mallas, I., Manoussakis, M., Mastrangelo, D., MacLachlan,  
559 C., McLean, P., Minami, A., Mladek, R., Nakazawa, T., Najm, S., Nie, Y., Rixen, M.,  
560 Robertson, A. W., Ruti, P., Sun, C., Takaya, Y., Tolstykh, M., Venuti, F., Waliser, D.,  
561 Woolnough, S., Wu, T., Won, D. J., Xiao, H., Zaripov, R., and Zhang, L.: The Subseasonal to  
562 Seasonal (S2s) Prediction Project Database, *Bull Am Meteorol Soc*, 98, 163-+,  
563 10.1175/Bams-D-16-0017.1, 2017.

564 Wang, B., and Xie, X.: Low-Frequency Equatorial Waves in Vertically Sheared Zonal Flow.  
565 Part I: Stable Waves, *J Atmos Sci*, 53, 449-467, 10.1175/1520-  
566 0469(1996)053<0449:lfewiv>2.0.co;2, 1996.

567 Wang, B., and Fan, Z.: Choice of south Asian summer monsoon indices, *Bull Am Meteorol*  
568 *Soc*, 80, 629-638, 10.1175/1520-0477(1999)080<0629:Cosasm>2.0.Co;2, 1999.

569 Wang, B., Wu, R. G., and Fu, X. H.: Pacific-East Asian teleconnection: how does ENSO  
570 affect East Asian climate?, *J Clim*, 13, 1517-1536, 2000.

571 Wang, B., Wu, R., and Li, T.: Atmosphere-Warm Ocean Interaction and Its Impacts on  
572 Asian-Australian Monsoon Variation\*, *J Clim*, 16, 1195-1211, 10.1175/1520-  
573 0442(2003)16<1195:aoiaii>2.0.co;2, 2003.

574 Wang, B., Kang, I.-S., and Lee, J.-Y.: Ensemble Simulations of Asian-Australian Monsoon  
575 Variability by 11 AGCMs\*, *J Clim*, 17, 803-818, 10.1175/1520-  
576 0442(2004)017<0803:esoamv>2.0.co;2, 2004.

577 Wang, B., Ding, Q. H., Fu, X. H., Kang, I. S., Jin, K., Shukla, J., and Doblas-Reyes, F.:  
578 Fundamental challenge in simulation and prediction of summer monsoon rainfall, *Geophys*  
579 *Res Lett*, 32, L15711, 10.1029/2005gl022734, 2005.

580 Wang, B.: *The Asian Monsoon*, Springer Science & Business Media, Praxis, New York, NY,  
581 USA, 2006.

582 Wang, B., Lee, J.-Y., Kang, I.-S., Shukla, J., Park, C. K., Kumar, A., Schemm, J., Cocke, S.,  
583 Kug, J. S., Luo, J. J., Zhou, T., Wang, B., Fu, X., Yun, W. T., Alves, O., Jin, E. K., Kinter, J.,  
584 Kirtman, B., Krishnamurti, T., Lau, N. C., Lau, W., Liu, P., Pegion, P., Rosati, T., Schubert,  
585 S., Stern, W., Suarez, M., and Yamagata, T.: Advance and prospectus of seasonal prediction:  
586 assessment of the APCC/CLIPAS 14-model ensemble retrospective seasonal prediction  
587 (1980-2004), *Clim Dyn*, 33, 93-117, 10.1007/s00382-008-0460-0, 2008a.

588 Wang, B., Wu, Z. W., Li, J. P., Liu, J., Chang, C. P., Ding, Y. H., and Wu, G. X.: How to  
589 measure the strength of the East Asian summer monsoon, *J Clim*, 21, 4449-4463,  
590 10.1175/2008jcli2183.1, 2008b.

591 Wang, B., Xiang, B., and Lee, J. Y.: Subtropical high predictability establishes a promising  
592 way for monsoon and tropical storm predictions, *Proc Natl Acad Sci U S A*, 110, 2718-2722,  
593 10.1073/pnas.1214626110, 2013.

594 Wang, B., Lee, J. Y., and Xiang, B. Q.: Asian summer monsoon rainfall predictability: a  
595 predictable mode analysis, *Clim Dyn*, 44, 61-74, 10.1007/s00382-014-2218-1, 2015.

596 Wu, R. G., Hu, Z. Z., and Kirtman, B. P.: Evolution of ENSO-related rainfall anomalies in  
597 East Asia, *J Clim*, 16, 3742-3758, 10.1175/1520-0442(2003)016<3742:Eoerai>2.0.Co;2,  
598 2003.

599 Wu, T. W., Song, L. C., Li, W. P., Wang, Z. Z., Zhang, H., Xin, X. G., Zhang, Y. W., Zhang,  
600 L., Li, J. L., Wu, F. H., Liu, Y. M., Zhang, F., Shi, X. L., Chu, M., Zhang, J., Fang, Y. J.,  
601 Wang, F., Lu, Y. X., Liu, X. W., Wei, M., Liu, Q. X., Zhou, W. Y., Dong, M., Zhao, Q. G., Ji,  
602 J. J., Li, L., and Zhou, M. Y.: An Overview of BCC Climate System Model Development and  
603 Application for Climate Change Studies, *J Meteorol Res-Prc*, 28, 34-56, 10.1007/s13351-  
604 014-3041-7, 2014.

605 Wu, Z. W., Wang, B., Li, J. P., and Jin, F. F.: An empirical seasonal prediction model of the  
606 east Asian summer monsoon using ENSO and NAO, *J Geophys Res Atmos*, 114, D18120,  
607 10.1029/2009jd011733, 2009.

608 Xiang, B., Wang, B., Yu, W., and Xu, S.: How can anomalous western North Pacific  
609 Subtropical High intensify in late summer?, *Geophys Res Lett*, 40, 2349-2354,  
610 10.1002/grl.50431, 2013.

611 Xiang, B. Q., Yu, W. D., Li, T., and Wang, B.: The critical role of the boreal summer mean  
612 state in the development of the IOD, *Geophys Res Lett*, 38, L02710, 10.1029/2010gl045851,  
613 2011.

614 Yang, S., Zhang, Z. Q., Kousky, V. E., Higgins, R. W., Yoo, S. H., Liang, J. Y., and Fan, Y.:  
615 Simulations and seasonal prediction of the Asian summer monsoon in the NCEP Climate  
616 Forecast System, *J Clim*, 21, 3755-3775, 10.1175/2008jcli1961.1, 2008.

617 Yim, S. Y., Wang, B., and Xing, W.: Prediction of early summer rainfall over South China by  
618 a physical-empirical model, *Clim Dyn*, 43, 1883-1891, 10.1007/s00382-013-2014-3, 2014.

619 Zhou, T., Wu, B., and Wang, B.: How Well Do Atmospheric General Circulation Models  
620 Capture the Leading Modes of the Interannual Variability of the Asian–Australian Monsoon?,  
621 *J Clim*, 22, 1159-1173, 10.1175/2008jcli2245.1, 2009.

622 Zhou, T. J., and Yu, R. C.: Atmospheric water vapor transport associated with typical  
623 anomalous summer rainfall patterns in China, *J Geophys Res Atmos*, 110, D08104,  
624 10.1029/2004jd005413, 2005.

625

Table 1. Details of the prediction systems investigated in this study.

System	Institute	Resolution		Non- Initialisation Members	Initialisation		Reference
		Atmospheric	Oceanic		Members	Type	
BCC-CSM1-1	Beijing Climate Center, China	T42L26	1lonx1.33lat L40	3	3	Full-field	Wu <i>et al.</i> (2014)
CanCM4	Canadian Centre for Climate Modelling and Analysis, Canada	T63L35	256 x 192 L40	10	10	Full-field	Arora <i>et al.</i> (2011)
GFDL-CM2p1	Geophysical Fluid Dynamics Laboratory, USA	N45L24	1lon x 0.33-1lat L50	10	10	Full-field	Delworth <i>et al.</i> (2006)
HadCM3	Met Office Hadley Centre, UK	N48L19	1.25x1.25 L20	10	10 + 10	Full-field Anomaly	andSmith <i>et al.</i> (2013)
MIROC5	Atmosphere and Ocean Research Institute, Japan	T85L40	256x192 L44	5	6	Anomaly	Tatebe <i>et al.</i> (2012)
MPI-ESM-LR	Max Planck Institute for Meteorology, Germany	T63L47	GR15 L40	3	3	Anomaly	Matei <i>et al.</i> (2012)

628 Table 2. Brief summaries of initialisation strategies used by modelling groups in the study. ECMWF: European Centre for Medium-Range Weather Forecasts;  
 629 GODAS: Global Ocean Data Assimilation System; NCEP: National Centers for Environmental Prediction; S: Salinity; SODA: Simple Ocean Data Assimilation; T:  
 630 Temperature. Initialised date shows the first initialised day of every prediction year.

system	Atmosphere	Ocean	Initialised date	Internet
BCC-CSM1-1	-	integration with ocean T nudged to SODA product above 1500 m	Ensemble 1: 1 <sup>st</sup> September Ensemble 2: 1 <sup>st</sup> November Ensemble 3: 1 <sup>st</sup> January	<a href="http://forecast.bccsm.ncc-cma.net/">http://forecast.bccsm.ncc-cma.net/</a>
CanCM4	ECMWF re-analysis	off-line assimilation of SODA and GODAS subsurface ocean T and S adjusted to reserve model T-S	1 <sup>st</sup> January	<a href="http://www.cccma.ec.gc.ca/">http://www.cccma.ec.gc.ca/</a>
GFDL-CM2p1	GFDL re-analysis	assimilates observations of T, S from World Ocean Database	1 <sup>st</sup> January	<a href="https://www.gfdl.noaa.gov/multidecadal-prediction-stream/">https://www.gfdl.noaa.gov/multidecadal-prediction-stream/</a>
HadCM3	ECMWF re-analysis	off-line ocean re-analysis product	1 <sup>st</sup> November	<a href="http://cerawww.dkrz.de/WDCC/CMIP5/">http://cerawww.dkrz.de/WDCC/CMIP5/</a>
MIROC5	-	integration using observational gridded ocean T and S	1 <sup>st</sup> January	<a href="http://amaterasu.ees.hokudai.ac.jp/">http://amaterasu.ees.hokudai.ac.jp/</a>
MPI-ESM-LR	NCEP re-analysis	off-line ocean hindcast forced with NCEP	1 <sup>st</sup> January	<a href="http://cerawww.dkrz.de/WDCC/CMIP5/">http://cerawww.dkrz.de/WDCC/CMIP5/</a>

631

632

633

634

635

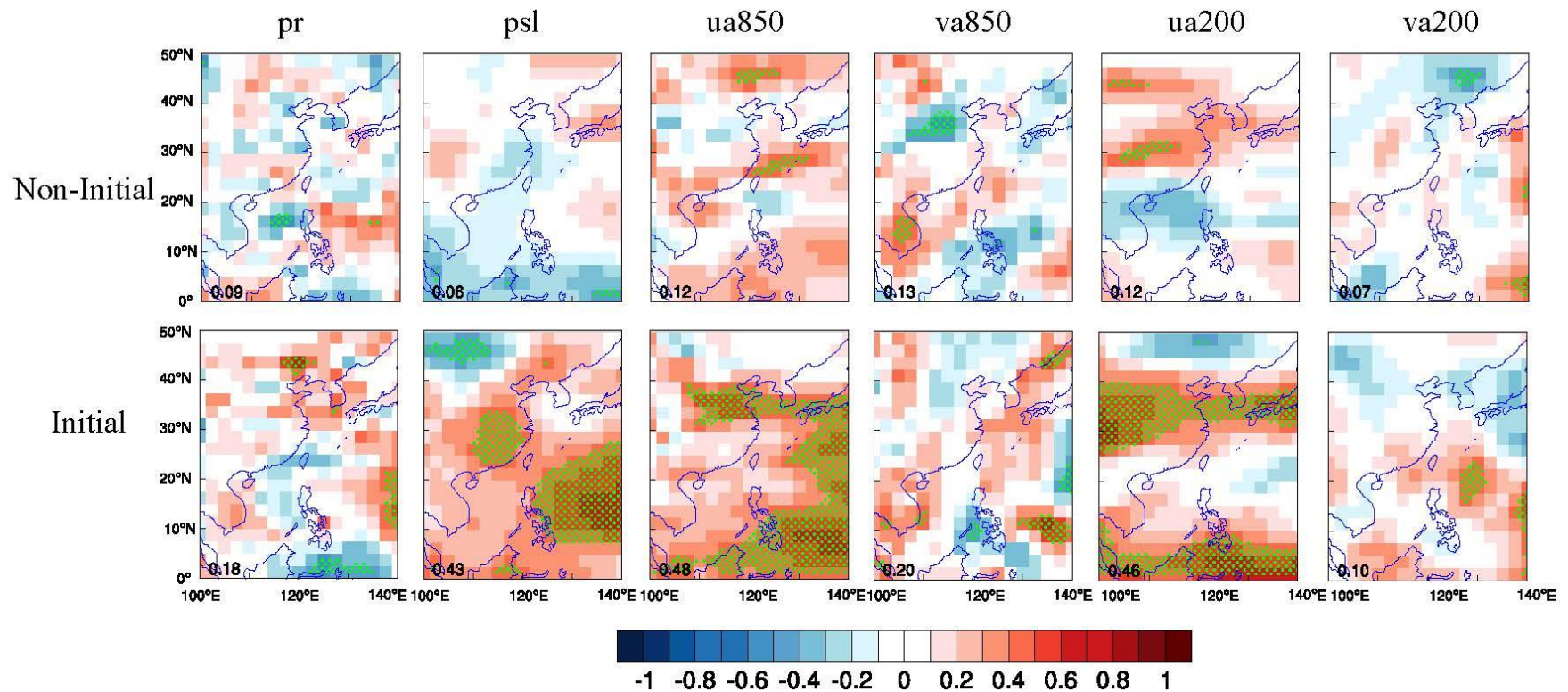
Table 3. Description of the six variables which contribute to the EASM. The abbreviation of these variables is followed to the guidelines of CMIP5.

variable	Standard name	Contribution to the EASM
pr	Precipitation	Precipitation distribution indicates the strength of EASM
psl	Mean sea surface pressure	Differences of mean sea surface pressure between land and ocean lead to EASM
ua850	Zonal winds over 850 hPa	A component of low-level cyclone which transports vapor from ocean to land
va850	Meridional winds over 850 hPa	As ua850, and contributes to Hadley's cell
va200	Meridional winds over 850 hPa	A component of upper-level Hadley's cell
ua200	Zonal winds over 850 hPa	As va200

636

637

638



639

640

641

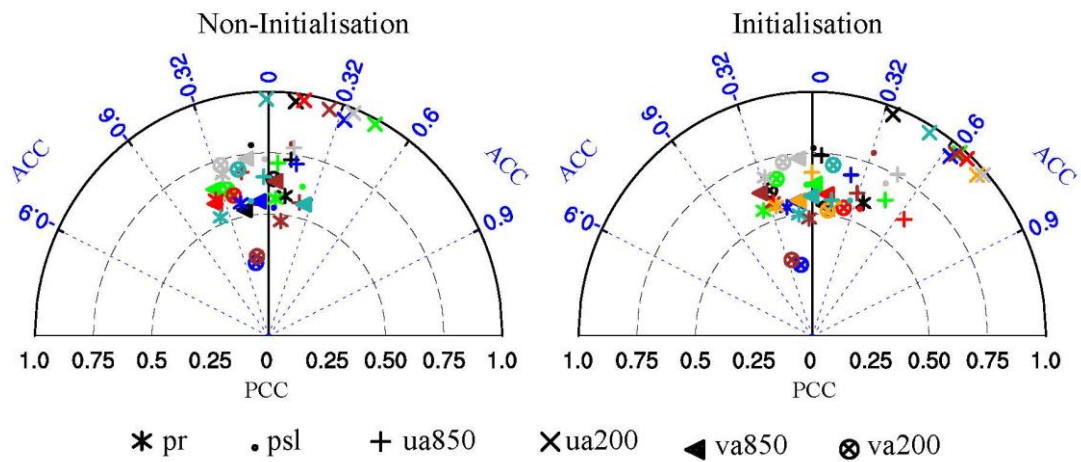
642

643

644

Fig. 1. Anomaly correlation coefficient of six variables (i.e. precipitation, mean sea level pressure, and winds over 850 hPa and 200 hPa) between multi-model ensemble mean and observations in non-initialisation and initialisation. The green dotted grids illustrate the significant level at 0.05. The number at lower left corner indicates the ratio of significant grid points to entire grids. The GPCP *wasis* employed as the reference data for precipitation (pr) while winds (i.e. ua850, va850, ua200 and va200) and mean sea level pressure (psl) *arewere* compared with ERA-Interim re-analysis.

645

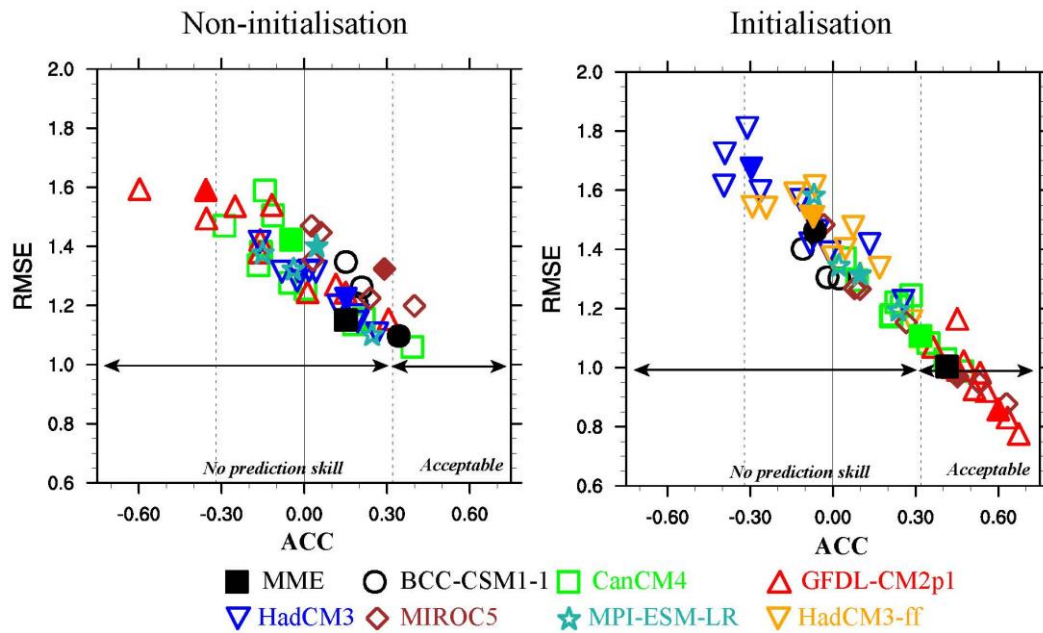


646

647 Fig.2. Taylor diagrams display of pattern (PCC) and temporal (ACC) correlation  
648 metrics of six variables between observation and model simulation in the EASM  
649 region (0-50°N, 100-140°E). Each coloured marker represents a model, *i.e.*, the BCC-  
650 CSM1-1 (black), the CanCM4 (green), the GFDL-CM2p1 (red), the HadCM3 (blue),  
651 the MIROC5 (brown), the MPI-ESM-LR (light-sea-blue), and the HadCM3-ff  
652 (orange).

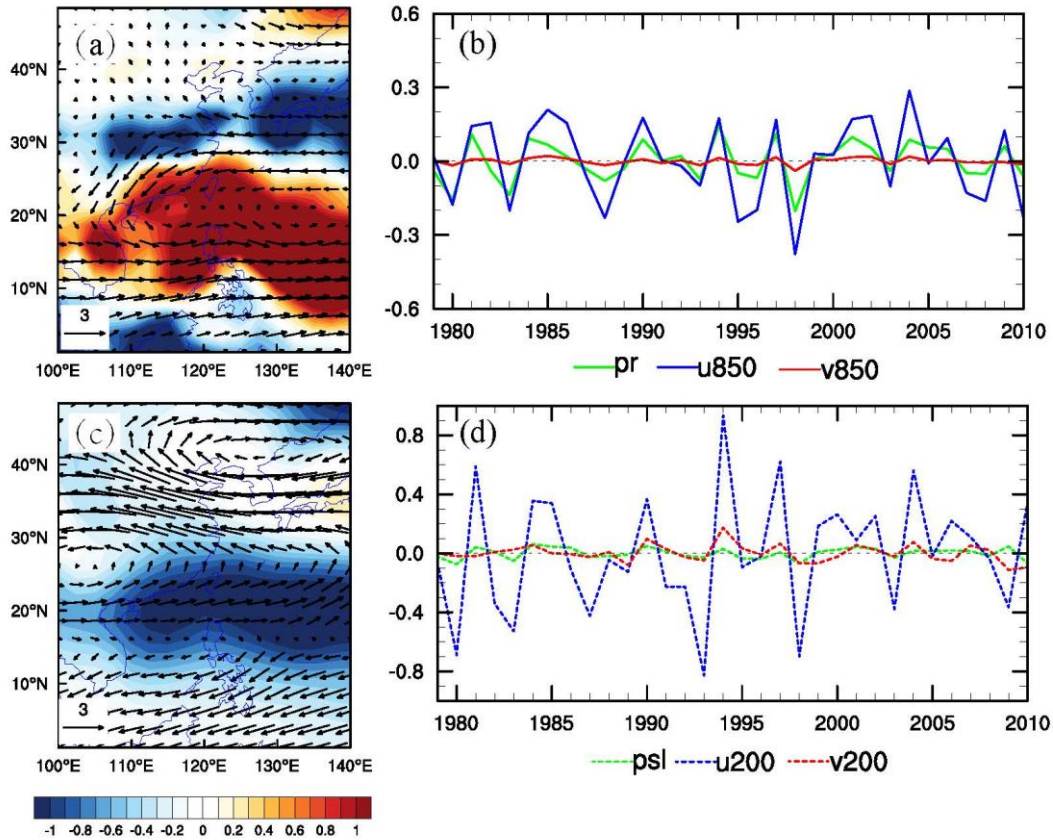
653





655

656 Fig. 3. Performance of the model ensemble member (hollow marker) and its ensemble  
 657 mean (solid marker) on the EASM index. The abscissa and ordinates are the anomaly  
 658 correlation coefficient (ACC) and the root-mean-square-error (RMSE), respectively.  
 659 The ~~observed-observation of~~ EASM index is calculated by zonal wind at 850 hPa  
 660 from the ERA-Interim re-analysis data. The black dot lines indicate the significant  
 661 level at 0.1. The vertical black line represents the correlation between the ~~simulating~~  
 662 ~~simulation~~ and the ~~observational of~~ EASM index is 0.



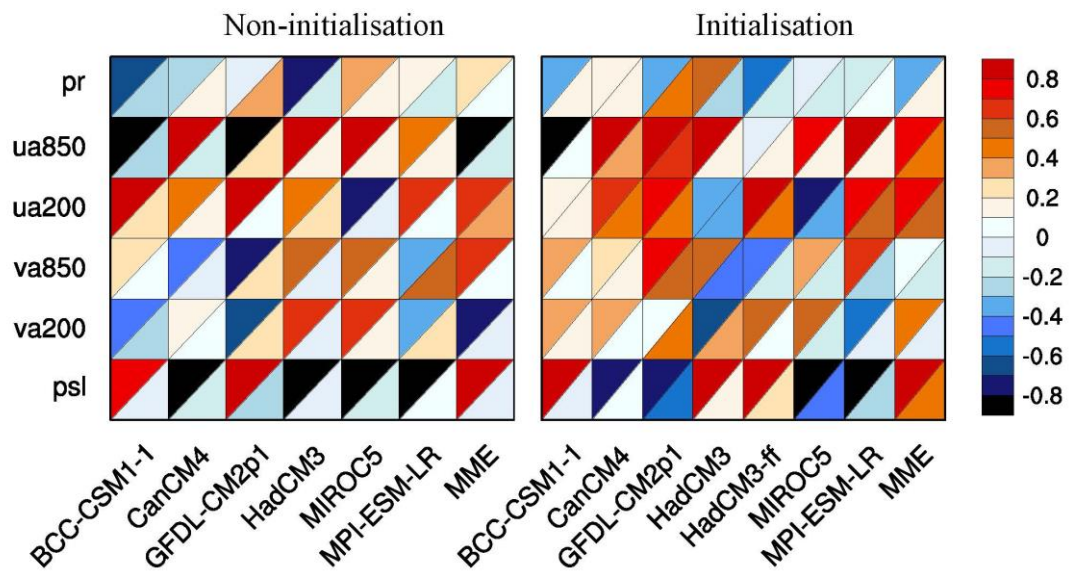
663

664 Fig. 4. Spatial distribution ~~of observational~~ of the first leading EOF mode of June-  
 665 July-August precipitation and winds over 850 hPa (a), mean sea level pressure and  
 666 winds over 200 hPa (c) and the associated principal component (PC; b, d). The GPCP  
 667 and the ERA-Interim data from 1979-2005 ~~are were~~ used for the EOF analysis in the  
 668 EASM domain.

669

670

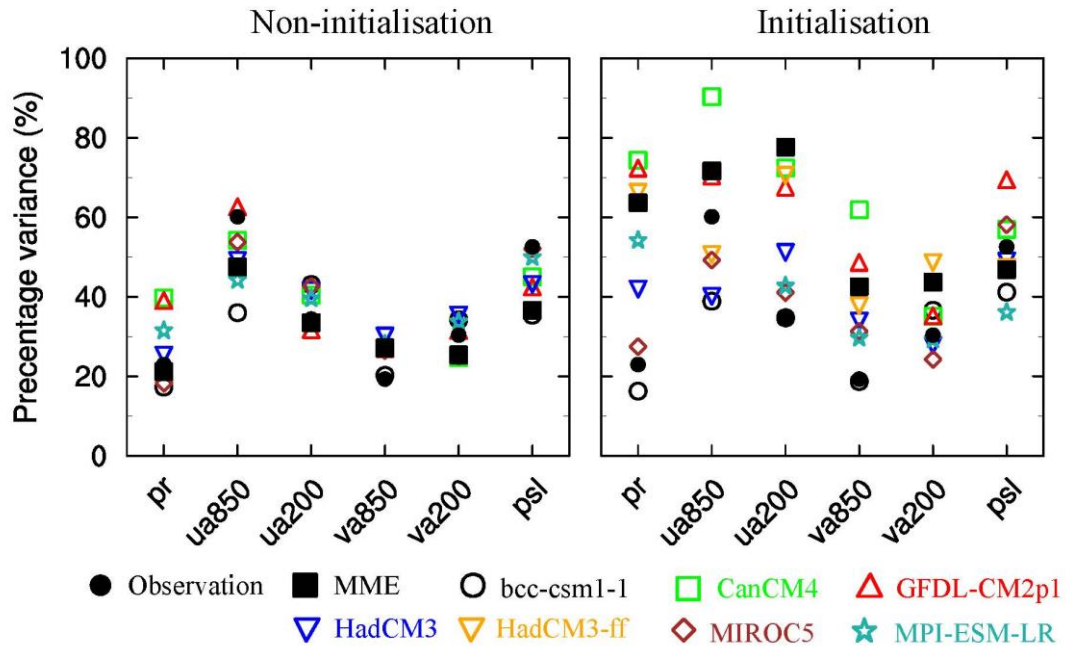
671



672

673 Fig. 5. Portrait diagram display of correlation metrics between the observation and the  
674 model simulation of the first lead EOF mode for the six fields in the non-initialisation  
675 (left) and the initialisation (right). Each grid square is split by a diagonal in order to  
676 show the correlation with respect to both the eigenvector (upper left triangle) and its  
677 associated principal components (lower right triangle) reference data sets.

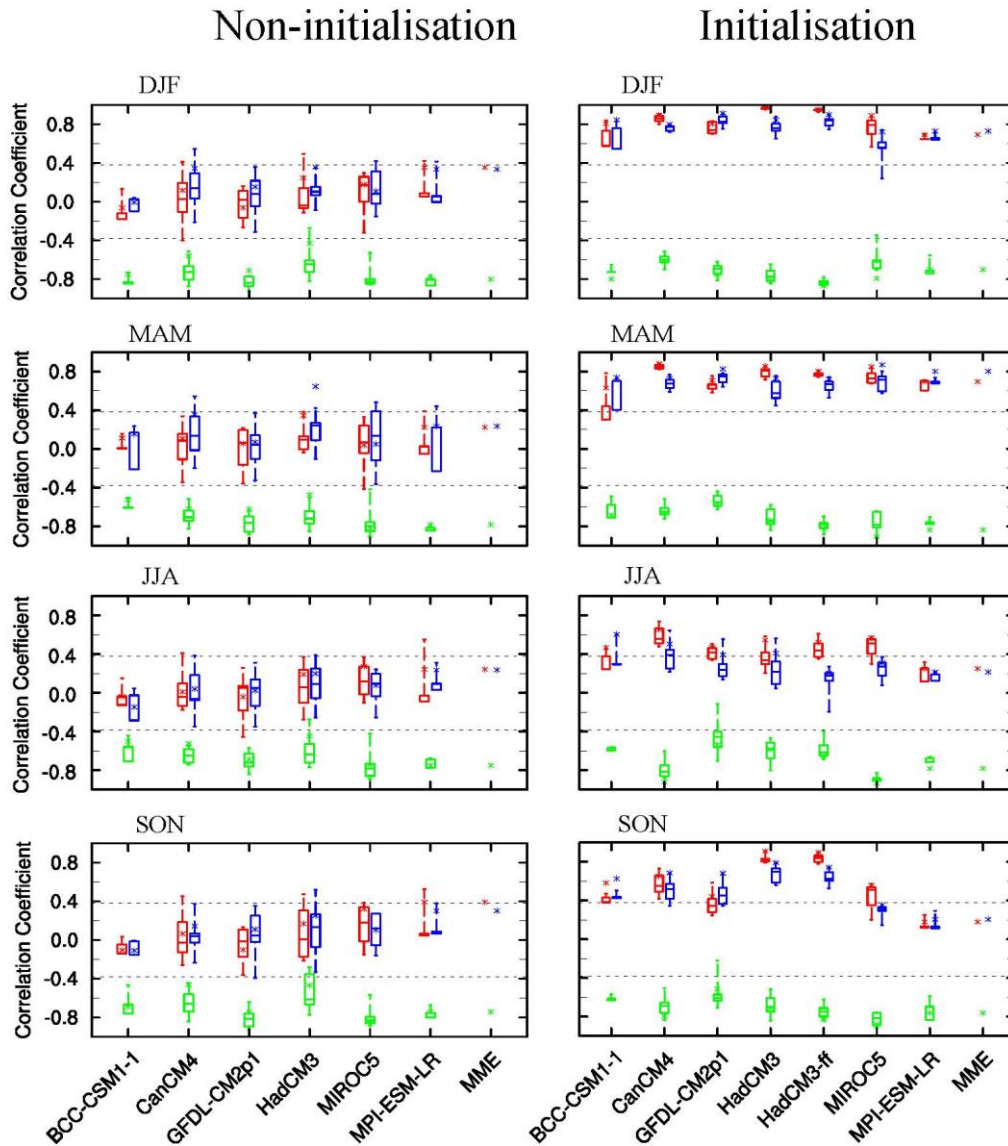
678



680

681 Fig. 6. Fraction variance (%) explained by the first EOF mode for six fields in the  
 682 non-initialisation (left) and the initialisation (right).

683



684

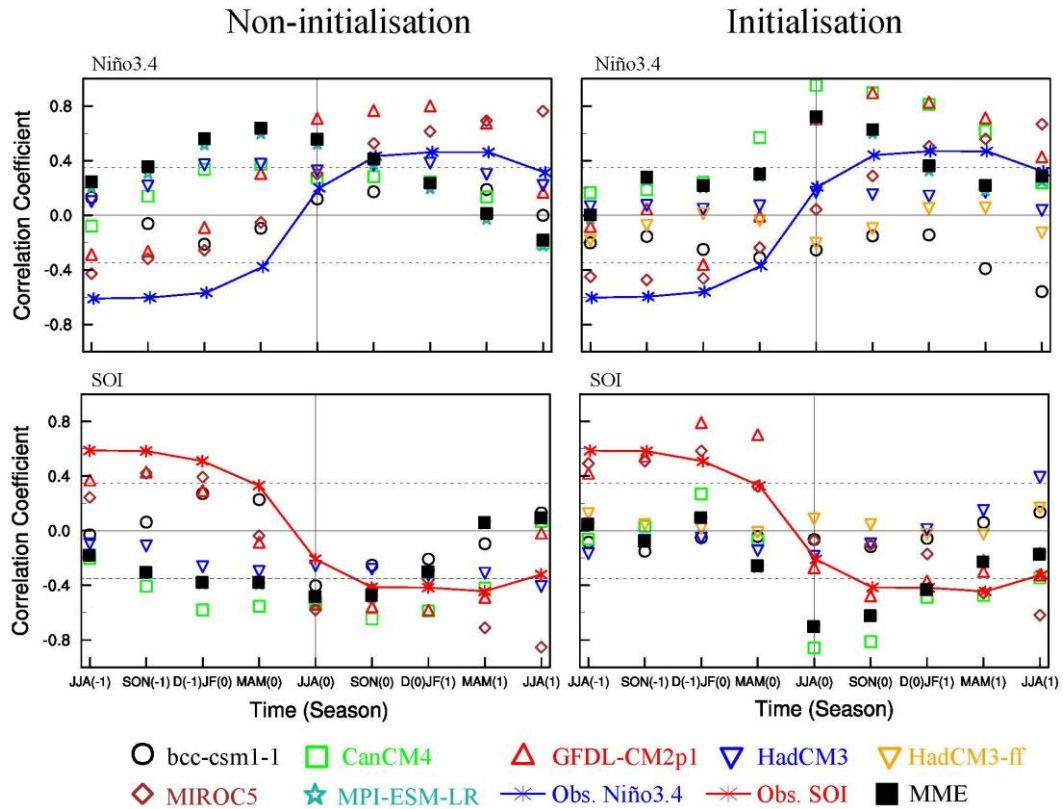
685 Fig. 7. Model prediction skill ~~in representing the observational of~~ Niño3.4 (red), ~~the~~  
 686 SOI (blue) from ~~the~~ DJF to SON in non-~~initialisation-initialised~~ (left) and ~~initialisation~~  
 687 ~~initialised~~ (right) ~~simulations~~. Green diagrams shows the correlation coefficient  
 688 between the model simulation~~ed of~~ Niño3.4 and the SOI. Box and whisker diagrams  
 689 shows ensemble mean of each model (asterisk), median (horizontal line), 25th and  
 690 75th percentiles (box), minimum and maximum (whisker). The two black dotted lines  
 691 indicate 0.05 significant level based upon Student's t-test.

692

693

694

695



696

697 Fig. 8. Lead-lag correlation coefficients between the EASM index and Niño3.4  
 698 (upper), and SOI (lower) in non-initialised simulations (left) and initialised ones  
 699 (right) for observation (marker line) and models (marker) from JJA(-1) to JJA(+1).  
 700 The two black dotted lines are 0.05 significant level based upon Student's t-test. The  
 701 vertical line represents JJA(0), where the simultaneous correlations between the  
 702 EASM index and Niño3.4, and SOI are shown.

703